5-31-2019

Voltage controlled magnetism in Cr2O3 based all-thin-film systems

Junlei Wang
University of Nebraska - Lincoln

Will Echtenkamp
University of Nebraska-Lincoln

Ather Mahmood
University of Nebraska - Lincoln

Christian Binek
University of Nebraska-Lincoln, cbinek@unl.edu

Journal of Magnetism and Magnetic Materials 486 (2019) 165262

Contents lists available at ScienceDirect

Journal of Magnetism and Magnetic Materials

journal homepage: www.elsevier.com/locate/jmmm

Voltage controlled magnetism in Cr_2O_3 based all-thin-film systems

Jun-Lei Wang, Will Echtenkamp, Ather Mahmood, Christian Binek*

Department of Physics and Astronomy, University of Nebraska-Lincoln, United States

ARTICLE INFO

Keywords:
Magnetoelectrics
Voltage-controlled magnetism
Exchange bias
Boundary magnetization
Spin Hall magnetoresistance
Anomalous Hall effect

ABSTRACT

Voltage-control of exchange biases through active selection of distinct domain states of the magnetoelectric and antiferromagnetic pinning layer is demonstrated for Cr_2O_3/CoPd heterostructures. Progress and obstacles towards an isothermal switching of exchange bias are discussed. An alternative approach avoiding exchange bias for voltage-controlled memory exploits boundary magnetization at the surface of Cr_2O_3 as voltage-controlled state variable. We demonstrate readout and switching of boundary magnetization in ultra-thin Cr_2O_3/Pt Hall bar devices where reversal of boundary magnetization is achieved via magnetoelectric annealing with simultaneously applied ± 0.5 V and 400 mT electric and magnetic fields.

1. Introduction

Spintronic device concepts utilizing the spin degree of freedom in magnetoelectric (ME) materials [1] have been a strong contender in the increasingly active research [2–8] of finding a suitable successor to the immensely successful complementary metal-oxide semiconductor (CMOS) systems. The (linear) ME effect refers to the induction of magnetization (polarization) with the application of an electric (magnetic) field was first observed in antiferromagnetic (AFM) insulators [9]. The strength of the induced magnetization/polarization is governed by a rank 2 ME susceptibility tensor, α_{ij}. Unlike the rank 2 magnetic and electric susceptibility tensors, α_{ij} has the unique property that its sign follows the sign of the AFM order parameter. In other words, in opposite AFM domains, the ME susceptibility has opposite signs, whereas the magnetic and electric susceptibilities remain the same. Rigorous symmetry arguments dictate that this effect can only take place in systems that are both time-reversal and space-inversion broken. A number of systems displaying this effect have been identified, including, e.g., Cr_2O_3 [10] and Fe_2TeO_6 [11]. It seems that the ME effect by itself could be a perfect candidate in spintronic applications because of its ability to manipulate spin alignments with an applied electric field, rather than an electric current. However, among the studied ME systems, none possesses strong enough ME coupling strength and/or high enough ordering temperature, Néel temperature (T_N), to be suitable for potential device applications independently. In addition, the linear ME effect is non-hysteretic. Hence there is no straight-forward path to use the linear ME effect for memory and switching. Investigations into fabricating novel device concepts utilizing the ME effect have to focus on using the ME effect in conjunction with other mechanisms, and increasing the ME ordering temperature. In the latter aspect, an increased Néel temperature in excess of 400 K [12] has been experimentally observed in B-doped Cr_2O_3 (chromia), which has a 307 K [10] ordering temperature when undoped.

Using magnetoelectricity as the key switching mechanism, different approaches have been proposed and studied for potential device applications [13]. Among those efforts, voltage controlled exchange bias (VCEB) systems have achieved notable success. He et al. achieved isothermal and bidirectional switching of the exchange bias of a Co/Pd multilayer structure on top of a chromia (0001) single crystals near room temperature later also confirmed in heterostructures using thick (in the range of 200–300 nm) chromia pinning layers [14–20]. These results utilized the net surface moment, known as “boundary magnetization” [21,22]. Boundary magnetization follows the sign of the domain state, and the AFM domains can be isothermally switched with combined application of electric and magnetic fields [23]. Here the sign of the exchange changes through switching of the out-of-plane boundary magnetization which couples via quantum mechanical exchange to the adjacent perpendicular anisotropic Co/Pt film. The orientation of the boundary magnetization follows the orientation of the switched AFM domain.

In order to utilize VCEB based on ME antiferromagnets in all thin film devices, improvements in many aspects, especially with respect to geometry and performance are deemed necessary. In this work, we discuss in detail the methodology and on-going challenges of achieving voltage-controlled magnetism in all-thin-film systems, and report the progress of realizing such systems. Finally, we identify that the approach of utilizing boundary magnetization as a direct switching mechanism can be more advantageous compared to systems with VCEB.

* Corresponding author .
E-mail address: cbinek@unl.edu (C. Binek).

https://doi.org/10.1016/j.jmmm.2019.165262
Received 30 January 2019; Received in revised form 9 April 2019; Accepted 1 May 2019
Available online 02 May 2019

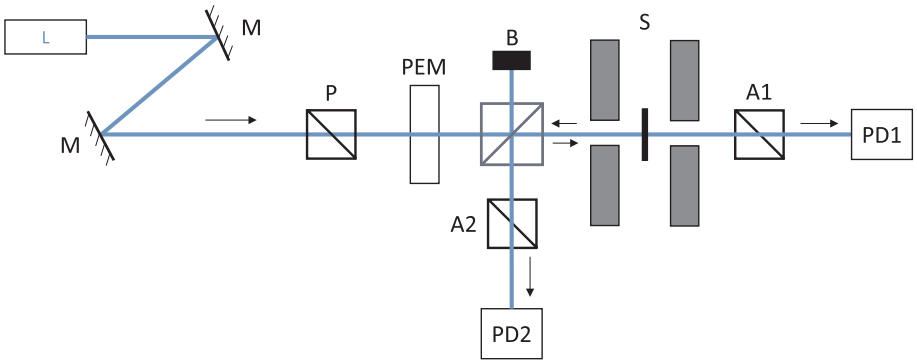

Fig. 1. Schematics of a magneto-optical setup which has the ability to detect magneto-optical Kerr and Faraday effects simultaneously. In practice, either branch of this setup can be disabled. L: laser. M: mirrors. B: beam block. P: polarizer. PEM: photo-elastic modulator. A1 & A2: analyzers. S: sample assembly. PD1 & PD2: photodetectors.

2. The magneto-optical methods of detecting voltage-controlled magnetism

The magneto-optical methods, especially Kerr and Faraday effects, provide a versatile, yet sensitive approach of studying both surface and bulk magnetism. Fig. 1 shows a setup diagram. It represents the various magneto-optical configurations used in this work. Optimized under the guidance outlined in Ref. [24], and by means of photo-elastic modulation and phase-sensitive lock-in amplifier detection, an absolute sensitivity of better than 10^{-5} degree can be achieved, as seen, e.g., from Ref. [25]. Our setups are designed to maximize the detection of the polar Kerr effect, which is sensitive to out-of-plane near-surface magnetization, with perpendicular incidence of the light on the sample surface. In addition, this design also retains the option to simultaneously detect bulk magnetization with the Faraday effect. The latter, accompanied with the ME effect, leads to a curious phenomenon where the electric field introduces a Faraday rotation [26]. The electric-field-induced Faraday effect allows for a straightforward and table-top apparatus of detecting the AFM order parameter and its orientation in ME antiferromagnets (Ref. [25] and Fig. 2). Specifically, the sign of the electric Faraday effect follows the sign of the AFM order parameter. The AFM domain switch is indicated by the reversal of the voltage-specific Faraday angle (Fig. 2, blue and red data in both panels), whereas a multi-domain is indicated by a diminished electric Faraday effect (Fig. 2, purple data in both panels).

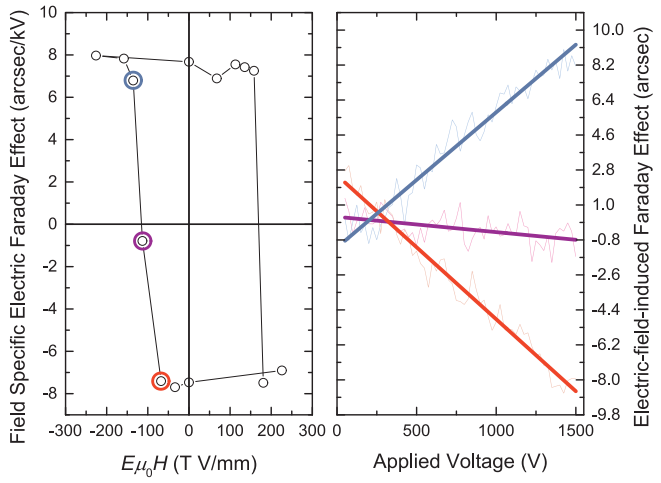

Fig. 2. Monitoring isothermal switching of AFM domain state in chromia (0001) single crystal, $5 \times 5 \times 0.5$ mm^3 with Pt electrodes, at $T = 305$ K, with electric-field-induced Faraday effect using light source of 980 nm wavelength. Left panel: Faraday rotation per applied voltage vs switching field product (circles). Applying electric and magnetic field simultaneously results in an asymmetric hysteresis-like loop indicating asymmetric switching thresholds. Right panel: three consecutive isothermal measurements of *E*-field induced Faraday rotation in zero applied magnetic field are displayed. Each isotherm is measured after a particular AFM domain state has been selected. The applied fields setting the negative single domain, multi domain, and positive single domain sate are highlighted in the left panel by red, purple, and blue circles, respectively. The data of the Faraday rotation vs. *E*-field in the right panel follow this color coding.

Next we outline the Jones matrix analysis [27], for our magneto-optical apparatus. Here the electric field of the light is expressed as a 1×2 vector, and a certain optical device (element) is expressed as a 2×2 matrix. Defining that the light is propagating along *z*-direction, with the *x*- and *y*-directions correspond to horizontal and vertical directions, respectively, we can express the optical elements as follows. For polarizers and analyzers,

$$\mathrm{P}(\theta) = \mathrm{A}(\theta) = \begin{pmatrix} \cos^2\theta & \sin\theta\cos\theta \\ \sin\theta\cos\theta & \sin^2\theta \end{pmatrix}, \tag{1}$$

where θ is the angle between the major transmission axis and the *x*-axis. Modulating along the *x*-axis, the photo-elastic modulator is expressed as,

$$\mathrm{PEM}(\delta, \omega) = \begin{pmatrix} e^{i\delta\sin\omega t} & 0 \\ 0 & 1 \end{pmatrix}, \tag{2}$$

where δ is the retardation amplitude, and ω is the modulation frequency. Since the absorption is relatively low, the sample can be expressed [24,28–30] as a Fresnel reflection matrix,

$$\mathrm{SR}(\Phi_K) = r_{ss}\begin{pmatrix} -1 & \Phi_K \\ \Phi_K & 1 \end{pmatrix}, \tag{3}$$

in Kerr (reflection) geometry and a rotation matrix,

$$\mathrm{ST}(\theta_F) = \begin{pmatrix} \cos\theta_F & -\sin\theta_F \\ \sin\theta_F & \cos\theta_F \end{pmatrix}, \tag{4}$$

in Faraday (transmission) geometry. Here r_{ss}, $\Phi_K = \theta_K + i\kappa_K$, θ_F are reflection coefficient, complex Kerr angle, and Faraday angle, respectively. Using the above Jones matrices, the reflected and transmitted light are expressed as,

$$E_R = \mathrm{A}_2(\phi')\mathrm{SR}(\Phi_K)\mathrm{PEM}(\delta, \omega)\mathrm{P}(\theta)E_I, \tag{5}$$

$$E_T = \mathrm{A}_1(\phi)\mathrm{ST}(\theta_F)\mathrm{PEM}(\delta, \omega)\mathrm{P}(\theta)E_I. \tag{6}$$

where θ, ϕ, ϕ', E_I are angle of the polarizer, analyzer at transmission light path, analyzer at reflection light path, and incident light, respectively. For optimal results [24,30], the following values are selected for the polarizer and analyzers, $\theta = \pi/4$, $\phi = 0$, and $\phi' = 0$. With these values, the photovoltaic signals detected by photodetectors PD1 and PD2 are,

$$I_{1,2f} = I_0 J_2(\delta)\sin 2\theta_F, \quad I_{2,2f} = 2r_{ss}^2 I_0 J_2(\delta)\theta_K, \tag{7}$$

on the second harmonics of the corresponding lock-in amplifiers. J_2 is the 2nd Bessel function of the first kind. The factor I_0 accounts for the initial signal intensity, the instrument factor of the photodetector, and other factors affecting the signal intensity. Using the lock-in signal

alone is suitable where proportionalities, i.e. $I \propto M$, suffice. Additional mechanisms, such as compensators, reference signals, or precision rotational stages are required for quantification of the magneto-optical angles.

3. Voltage controlled exchange bias in all-thin-film systems

Because α_{ij} has opposite signs for opposite domains the ME effect is at its maximum in a single domain state. Selecting a domain state in ME antiferromagnets, e.g., chromia, employs a protocol known as ME annealing [31], where electric and magnetic fields are applied simultaneously when cooling down from paramagnetic (PM) to AFM ordering. The sign of the selected AFM domain depends on the relative sign between the annealing fields. If cooling from above to below the AFM ordering temperature without applying any external fields, the two 180 degree domains will be formed as the long-range AFM order establishes. The two energetically degenerate domains will each occupy, statistically speaking, equal amount of sample volume. In such a multi-domain state, the integral bulk ME effect will be nullified, e.g., the diminished electric-field-induced Faraday effect in the multi-domain state (Fig. 2, purple line of right panel). However, with the overlaying exchange heterostructures, e.g., a Co/Pd multilayer, opposite exchange biases from opposite AFM domain can coexist and, if so, are reflected in the hysteresis loop.

In Fig. 3, we demonstrate the coexistence of exchange biases with opposite signs of a Co/Pd multilayer on a Cr_2O_3 (0001) film of 250 nm, simultaneously detected by magneto-optical Kerr (red) and Faraday (blue) effects. To achieve the simultaneous detection of both geometries, a wavelength of 785 nm is selected such that both optical branches have acceptable intensities. The protocol of the measurement is as follows: the system is cooled down from $T = 320\ \mathrm{K} > T_N$ to $T = 295\ \mathrm{K} < T_N$ without applying any external fields, and therefore a multi-domain state is formed in the chromia layer. Statistically, the two opposite domains should occupy equal areas on a macroscopic level, however, due to the limited probing area of our magneto-optical method, one domain is slightly favored over the other. This multi-domain state resulted in a split behavior of exchange bias (Fig. 3, top left panel), i.e., the hysteresis loop will follow first one type of the exchange bias loop and then follow the other after a quick transition. This behavior is known for other EB systems as well, e.g., in Fe/FeF_2 [32]. At $T = 295\mathrm{K}$, both domains have a sizeable EB of $\mu_0 H_{EB} \approx 30\mathrm{mT}$. As the temperature increases, the EB gradually reduces and finally completely disappear as chromia transits into PM phase at $T \approx$ 307K (Fig. 3).

The key advancement towards VCEB in all-thin-film system is the ability to select a single domain state in the ME chromia layer. Nevertheless, applying an electric field strength sufficient for ME annealing across chromia thin films is challenging, as chromia in thin film geometry, even samples with substantial thickness of hundreds of nanometers, cannot sustain its bulk dielectric property. Structural defects and lattice mismatches between adjacent layers are commonly viewed responsible for such difficulties [19,20]. Many approaches have been suggested to resolve this, among which the approach with reduced sample area has proven to be effective [33]. The smaller sample area statistically reduces the possibility of defect occurrence, and also aligns with device applications where areas are expected to be on the order of nm^2. In turn, the smaller sample area also reduces the sample volume, which makes selecting AFM domain with only the magnetic field possible [34,35].

Complete shifts of exchange bias loops are essential to realize ultra-low power non-volatile magnetic memory and other devices based on the building block of VCEB. Fig. 4 shows the fully shifted hysteresis loop as a result of magnetic field cooling on a reduced area $Cr_2O_3/Pd/(Co/Pd)_2$ exchange bias heterostructure. Lithographic patterning and Ar ion etching was used to structure the Co/Pd top layer in a circle with a diameter of 120 μm. Ti/Au electrodes are then deposited through a second step of lithography. Before the deposition of electrodes, a 40 nm thick HfO_2 layer was introduced as a spacer between electrodes and underlying chromia to minimize leakage. Without applying any electric field, the sampled is cooled from above T_N (320 K) to below (280 K) with a magnetic field of 0.7 T. Hysteresis loop of this field cooled

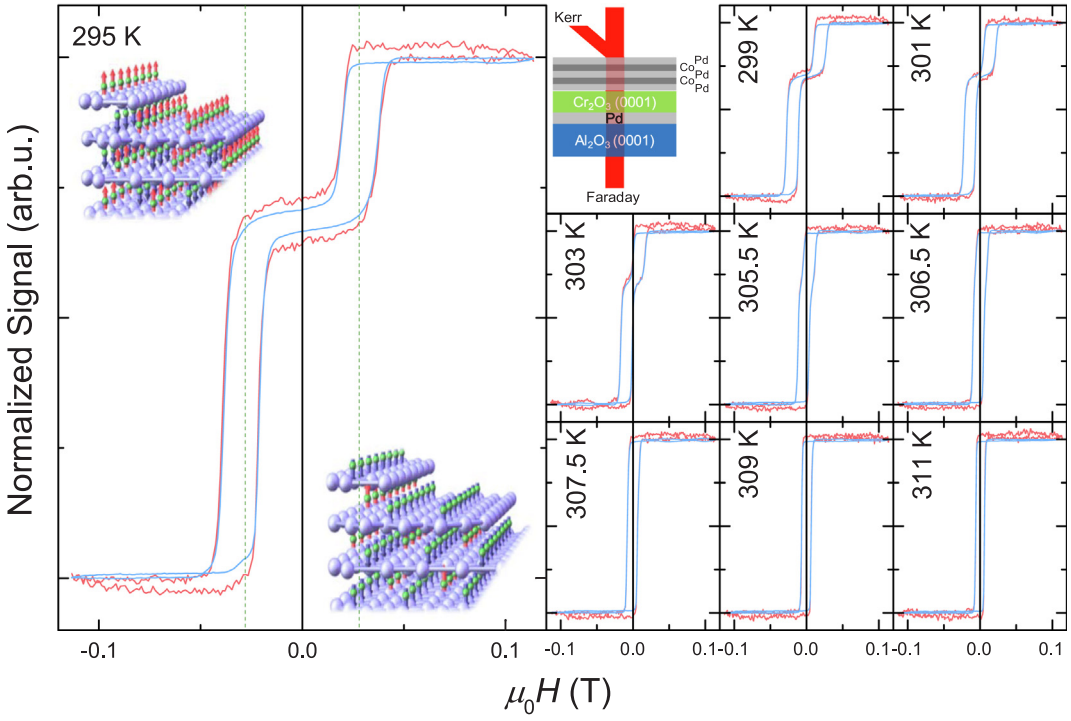

Fig. 3. Exchange bias hysteresis loops of a Co/Pd multilayer on top of a multi-domain Cr_2O_3 (0001) layer of 250 nm. This structure is illustrated in the top middle inset. Left panel shows the coexistence of exchange biases with opposite signs over the corresponding domains of Cr_2O_3. Right panels show the evolution of the exchange biases as temperature changes from $T = 295\ \mathrm{K} < T_N$ to $T = 311\ \mathrm{K} > T_N$.

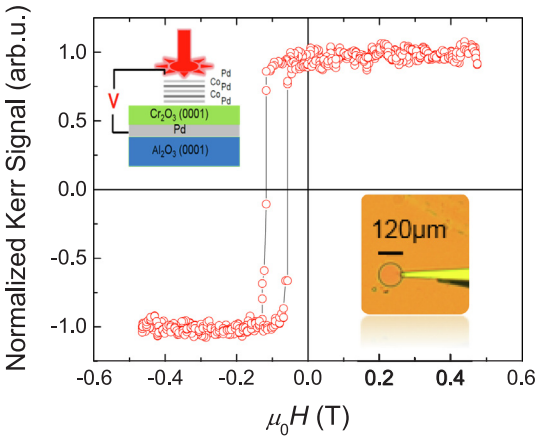

Fig. 4. Exchange bias hysteresis loop of a lithographically patterned Co/Pd multilayer on top of Cr_2O_3 (0001) film of 300 nm, detected by polar Kerr effect using a focused 532 nm laser. The sample surface has a diameter of 120 μm, indicated by the microscopy image of the inset. The sample was cooled from 320 K to 280 K with applied magnetic field $\mu_0 H = 0.7$ T and no electric field. This data is measured at 295 K, with a fully shifted hysteresis loop and an exchange bias of $\mu_0 H_{EB} \approx 110$ mT.

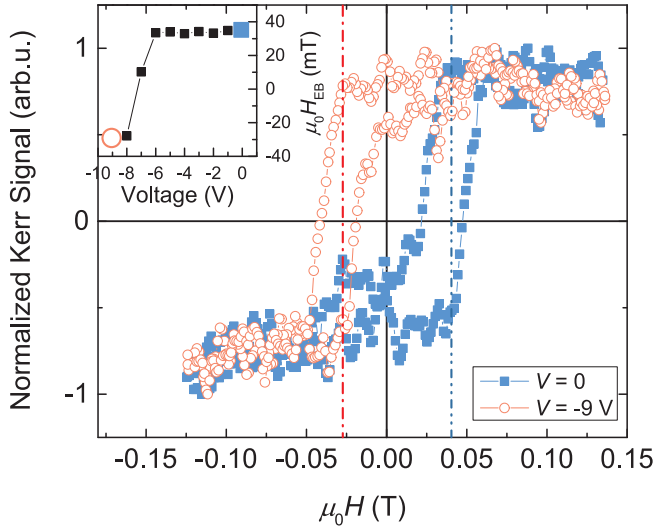

Fig. 5. Switching of exchange bias in a chromia based all-thin-film exchange bias system, as detected by polar Kerr effect using laser of 532 nm wavelength. Patterned Pd(20 nm)/Cr_2O_3(500 nm)/Pd(1 nm)/(Co(0.6 nm)/Pd(1 nm))$_2$ heterostructure of 90 × 90 μm^2 surface area is prepared with positive exchange bias $\mu_0 H_{EB} \approx$ 40mT (blue squares). Next switching fields of 0.7 T and −9 V are applied. After removal of the switching fields, a negative exchange bias $\mu_0 H_{EB} \approx$ −30mT is observed (red hollow circles) in the likewise fully shifted hysteresis loop. Inset shows exchange bias as a function of the switching voltage applied, data shown in the main frame is represented by the same symbol in the inset.

sample is measured by polar Kerr effect at $T = 295$K, using a focused 532 nm laser. The result shows a fully shifted loop with an exchange bias of $\mu_0 H_{EB} \approx 110$mT, indicating the chromia layer was annealed to a single domain state. These lithographically patterned samples paved way to VCEB with their improved electric properties and ability to anneal with applied magnetic field alone to single domain states. Next we employ the ME switching on a similarly patterned, 90 × 90 μm^2 surface area Pd/Cr_2O_3/Pd/(Co/Pd)$_2$ EB system, where the 20 nm bottom Pd layer is used as the electrode. The results are shown in Fig. 5. Similar to what is done in Fig. 4, the sample was prepared with a positive EB. Next, the initial switching magnetic and electric fields of 0.7 T and 0 V are simultaneously applied to the sample. After the fields are pulsed the hysteresis is measured (Fig. 5, blue solid squares) and the EB $\mu_0 H_{EB} \approx$ 40 mT is calculated, the process is repeated for electric fields up to −9 V. After switching fields of 0.7 T and −9 V are applied the sample is indeed switched, indicated by another fully shifted hysteresis loop with a negative EB $\mu_0 H_{EB} \approx$ 30mT (Fig. 5, red hollow circles). The result of Fig. 5 demonstrates a voltage controlled, isothermal switching of chromia based EB system. Nevertheless, this switching is unidirectional,as the switching back from the negative EB to positive couldn't be achieved on this sample, if maintaining the sign of the switching magnetic field. A constant sign of magnetic field during the ME switching is a prerequisite for true voltage controlled switching because a constant magnetic field can be provided for instance by a permanent magnet layer.

We consider this difficulty of bidirectional switching of exchange bias as twofold. First, the intrinsic switching threshold of chromia is asymmetric. Even in pure chromia, a little asymmetry in switching threshold is known (Fig. 2 left panel, and in [14,23]), the exchange coupling between the overlying EB ferromagnet and the AFM layer will further differentiate on the opposite switching directions [20,36]. More importantly, however, the interface exchange coupling energy density, J, introduces another term for the switching fields to overcome,

$$F_{EX} = \frac{J m_{BM} S_{FM}}{t_{AFM}} \tag{8}$$

where m_{BM} is the boundary magnetization, S_{FM} is interface ferromagnetic spins, and t_{AFM} is the thickness of the AFM layer [20,36,37]. Depending on the sign of J, F_{EX} can either promote or hinder the switching to one direction compared to the other. In addition, the existence of a finite AFM remnant magnetization [34,35,38], M_{AFM}, further lifts the degeneracy between the switching electric and magnetic fields. Here M_{AFM} alters the energy gained by applying the switching fields to

$$F_{sw} = \left(\alpha_{33} E + \frac{M_{AFM}}{t_{AFM}}\right) H, \tag{9}$$

where $\alpha_{33} = \alpha_{\parallel}$ is the parallel ME susceptibility. Taking both factors into account, with a constant magnetic field, the most favored switching electric field differs from the most unfavored field with,

$$\Delta E_{SW} = \frac{2}{\alpha_{\parallel}} \left(\frac{J S_{FM} m_{BM}}{t_{AFM} H} + \frac{M_{AFM}}{t_{AFM}} \right). \tag{10}$$

This difference could have made the electric field needed for our sample to reverse switching to exceed its breakdown voltage.

4. Direct voltage control of boundary magnetization

As shown above, the VCEB is seemingly a viable approach to achieve voltage controlled switching. Nevertheless, there are many challenges to overcome before VCEB could be suitable for potential device applications. For device applications, the switching mechanism must be complete bidirectional, isothermal, taking place at, or preferably well above, room temperature, and in all-thin-film and scalable geometry all at once. Experimental realizations of such VCEB systems are scarce at best. For practical implementations, it will be in particular necessary to substantially reduce the applied magnetic field. In principle, the magnetic field used for switching can be arbitrarily small because it is the product of magnetic and electric field that, in first approximation, determines the switching of the antiferromagnet. A practical example of this is given in Ref. [21], which used the earth's magnetic field in a magnetoelectric annealing experiment. For isothermal electric switching experiments in thin films, the situation is more difficult, reducing the switching magnetic field, requires the electric field to be increased accordingly. Since the dielectric breakdown of the chromia thin films is one of the primary difficulties faced in these types of experiments, it is often not feasible to do this. Despite these difficulties switching of the remnant magnetization has been

demonstrated in Ref. [19].

Also, as discussed in the previous section, the exchange coupling between the AFM and FM layers introduces additional energy needed to achieve bidirectional switching. Overcoming this energy is made more challenging because the ME energy scales with the volume and thus is reduced in thin films, and the specific ME susceptibility tends to be reduced in thin films as well [39]. To compensate for the reduced volume and reduced ME susceptibility one would have to apply higher electric fields. This option is, however, limited due to dielectric breakdown. This makes the VCEB based device concepts a difficult compromise; on one hand, FM structures provide higher signal level (easy to read), on the other hand, exchange coupling requires higher energy to switch (difficult to write).

In many novel device concepts, lowering of the energy consumption in both reading and writing process is prioritized. Therefore, ME device concepts without FM-AFM coupling are proposed. One of such concepts [40] directly manipulates the boundary magnetization, at the same time using PM metals with high stoner susceptibility, such as Pd or Pt, as both electrodes and signal enhancement through proximity effects [41,42]. A proof-of-principle magneto-optical detection of the inducted magnetization in the Pt layer on a bulk Cr_2O_3 (0001) surface is shown in Ref. [43], where the remnant magnetization was detected as a function of temperature and a clear onset at T 307 K $\approx T_N$ is observed. Here, with the progress to diminish the electric leaking in chromia thin films as outlined in [33], we demonstrate the promising scalability of such concept by the study conducted on an ultra-thin 20 nm chromia film with a 3 nm Pt overlayer (Fig. 6). The sample is field cooled applying 0.4 T magnetic field and either a −0.5 V (Fig. 6 blue curve) or 0.5 V (Fig. 6 red curve), from 320 K to 290 K. The average leakage current associated with 0.5 V is about $2.6 \times 10^{-7}A$ over a sample area of $80\mu m^2$. The fields are removed prior to measurement. An anomalous Hall effect (AHE)-like signal is measured on the Pt overlayer on zero-field heating. There are competing mechanisms discussed in the literature which can contribute to the AHE-like voltage signal, $V_{xy,}$ and its dependence on temperature and magnetic field H_z oriented normal to the *xy*-plane of the Hall bar. A proximity effect has been discussed [44] where boundary magnetization induces magnetization in the adjacent heavy metal (HM) layer via an exchange field. Although this mechanism seems plausible for chromia/Pt quantitative estimates show [45] that the proximity effect is typically negligible compared to spin Hall magnetoresistance (SMR). This is confirmed in chromia/Ta [46] and YIG/Pt [47]. The favorable mechanism SMR results from the combined action of the spin Hall effect, i.e., the generation of a spin current in the HM due to charge transport in the presence of spin–orbit interaction, and the inverse spin Hall effect, i.e., the conversion of a spin current into a charge current [48]. An AHE-like signal occurs in the context of SMR if the imaginary part of the spin mixing conductance is non zero. Despite the fact that many feature of magnetoresistance in chromia/Pt can be understood on the basis of SMR [49], it is increasingly apparent that the current theoretical framework of SMR is not sufficient to explain all experimental observations. There is increasing evidence that the complex mixing conductance, which is currently treated as a constant, must be generalized into a complex function of temperature and magnetic field. Details of this are currently under investigation and will be published elsewhere. It is important to stress here, that independent of the details of the mechanism the AHE-like signal, it is a proxy of the AFM boundary magnetization and can serve to detect its orientation and magnitude [40,42]. The Hall voltage measured on heating in zero applied magnetic field indicates a clear onset of boundary magnetization and thus AFM order in chromia. The sign of the remnant magnetization is determined by the sign of the *EH*-product applied during field cooling. Note here, the measured signal is suffering from well-known parasitic signal offsets due to imperfect device geometry [42]. This offset can be avoided altogether when a spinning current technique is employed. This was not the case in the displayed measurements and hence the absence of merging of the two data sets for different orientation of the AFM order parameter. It may seem remarkable that the onset of boundary magnetization takes place close to bulk ordering temperature (~307 K) in an AFM film as thin as 20 nm. However, in the case of chromia 20 nm is still well above the thickness regime where finite size effects reduce the Néel temperature [50] in accordance with previous findings indicating that apparent finite-size effects are not due to confinement of the AFM correlation length but rather caused by defects which vary between different growth methods [39].

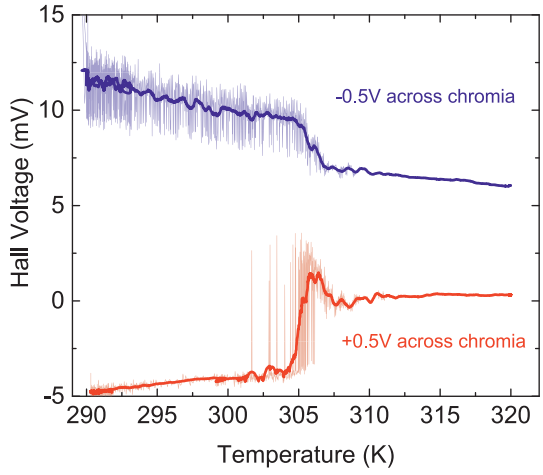

Fig. 6. Remnant anomalous Hall effect signal of Pt overlayer (3 nm) on a 20 nm Cr_2O_3 thin film. The sample is field cooled with plus (red) or minus (blue) 0.5 V voltage and 0.4 T magnetic fields, from 320 K to 290 K. The measurements are taken during zero-field heating.

The fact that a sizeable induced magnetization resulted from an ultra-thin chromia film reinforces the concept that boundary magnetization is responsible for this effect. Additionally, being able to observe this effect with such small voltage (about 10 times smaller than reported in Ref. [40] with similar electric field) and a temperature behavior largely in line with the expected AFM order parameter behavior has promising implications for the realization of scalable devices.

5. Conclusion

Magnetoelectric materials, such as chromia, provide an isothermal voltage-controlled switching mechanism that can be used in novel energy efficient post-CMOS device concepts. Voltage controlled exchange bias is seen as a viable approach in realizing such concepts. In this work, progress in all-thin-film voltage controlled exchange bias systems is demonstrated with promising implications for device applications. Yet, challenges with respect to operation temperature and switching in scaled devices remain. To overcome these problems, we implement a device concept with reduced complexity which eliminates ferromagnetic constituents. It rather utilizes boundary magnetization as voltage-controllable state variable. We demonstrate reversal of boundary magnetization through magnetoelectric annealing with unprecedented low applied voltages as small as ± 0.5 V across a 20 nm chromia thin film. Sensing takes place with the help of a Pt Hall bar. This result shows evidence for scalability of energy efficient magnetoelectric devices for memory and logic.

Acknowledgement

This work was supported in part by Antiferromagnetic Magnetoelectric Memory and Logic (AMML), one of centers in nCORE as task 2760.001, a Semiconductor Research Corporation (SRC) program sponsored by the NSF through ECCS 1740136 and through the Nebraska Materials Research Science and Engineering Center (MRSEC)

(grant No. DMR-1420645). The research was performed in part in the Nebraska Nanoscale Facility: National Nanotechnology Coordinated Infrastructure and the Nebraska Center for Materials and Nanoscience, which are supported by the National Science Foundation under Award ECCS: 1542182, and the Nebraska Research Initiative.

Appendix A. Supplementary data

Supplementary data to this article can be found online at https://doi.org/10.1016/j.jmmm.2019.165262.

References

[1] J.A. Kelber, C. Binek, P.A. Bowden, K. Belashchenko, Magneto-Electric Voltage Controlled Spin Transistors, in: S. United (Ed.), QUANTUM DEVICES LLC, University of North Texas, US20140231888A1, 2014.
[2] D.E. Nikonov, I.A. Young, Overview of beyond-CMOS devices and a uniform methodology for their benchmarking, Proc. IEEE 101 (2013) 2498–2533, https://doi.org/10.1109/JPROC.2013.2252317.
[3] D.E. Nikonov, G.I. Bourianoff, T. Ghani, Proposal of a spin torque majority gate logic, IEEE Electron Device Lett. 32 (2011) 1128–1130, https://doi.org/10.1109/LED.2011.2156379.
[4] A.C. Seabaugh, Q. Zhang, Low-voltage tunnel transistors for beyond CMOS logic, Proc. IEEE 98 (2010) 2095–2110, https://doi.org/10.1109/JPROC.2010.2070470.
[5] S.O. Koswatta, M.S. Lundstrom, D.E. Nikonov, Performance comparison between p-i-n tunneling transistors and conventional MOSFETs, IEEE Trans. Electron Devices 56 (2009) 456–465, https://doi.org/10.1109/TED.2008.2011934.
[6] T. Fischer, M. Kewenig, D.A. Bozhko, A.A. Serga, I.I. Syvorotka, F. Ciubotaru, C. Adelmann, B. Hillebrands, A.V. Chumak, Experimental prototype of a spin-wave majority gate, Appl. Phys. Lett. 110 (2017) 152401, , https://doi.org/10.1063/1.4979840.
[7] S. Luo, M. Song, X. Li, Y. Zhang, J. Hong, X. Yang, X. Zou, N. Xu, L. You, Reconfigurable Skyrmion logic gates, Nano Lett. 18 (2018) 1180–1184, https://doi.org/10.1021/acs.nanolett.7b04722.
[8] Z. Sun, E. Ambrosi, A. Bricalli, D. Ielmini, Logic computing with stateful neural networks of resistive switches, Adv. Mater. 30 (2018) 1802554, https://doi.org/10.1002/adma.201802554.
[9] D.N. Astrov, The magnetoelectric effect in antiferromagnetics, Sov. Phys. JETP-USSR 11 (1960) 708–709.
[10] D.N. Astrov, Magnetoelectric effect in chromium oxide, Sov. Phys. JETP-USSR 13 (1961) 729–733.
[11] S. Buksphan, R. Hornreic, E. Fischer, Magnetoelectric and Mossbauer studies of Fe_2TeO_6, Solid State Commun. 10 (1972) 657, https://doi.org/10.1016/0038-1098(72)90580-7.
[12] M. Street, W. Echtenkamp, T. Komesu, S. Cao, P.A. Dowben, C. Binek, Increasing the Néel temperature of magnetoelectric chromia for voltage-controlled spintronics, Appl. Phys. Lett. 104 (2014) 222402, , https://doi.org/10.1063/1.4880938.
[13] C. Binek, B. Doudin, Magnetoelectronics with magnetoelectrics, J. Phys.-Condens. Mat. 17 (2005) L39–L44, https://doi.org/10.1088/0953-8984/17/2/L06.
[14] X. He, Y. Wang, N. Wu, A.N. Caruso, E. Vescovo, K.D. Belashchenko, P.A. Dowben, C. Binek, Robust isothermal electric control of exchange bias at room temperature, Nat. Mater. 9 (2010) 579–585, https://doi.org/10.1038/nmat2785.
[15] W. Echtenkamp, C. Binek, Electric control of exchange bias training, Phys. Rev. Lett. 111 (2013), https://doi.org/10.1103/PhysRevLett.111.187204.
[16] P. Borisov, A. Hochstrat, X. Chen, W. Kleemann, C. Binek, Magnetoelectric switching of exchange bias, Phys. Rev. Lett. 94 (2005), https://doi.org/10.1103/PhysRevLett.94.117203.
[17] P.A. Dowben, C. Binek, D.E. Nikonov, Nanoscale Silicon Devices, CRC Press, Boca Raton, FL, 2015.
[18] W. Kleemann, C. Binek, Multiferroic and magnetoelectric materials, Springer Trac. Mod. Ph. 246 (2013) 163–187, https://doi.org/10.1007/978-3-642-32042-2_5.
[19] T. Ashida, M. Oida, N. Shimomura, T. Nozaki, T. Shibata, M. Sahashi, Isothermal electric switching of magnetization in Cr2O3/Co thin film system, Appl. Phys. Lett. 106 (2015) 132407, , https://doi.org/10.1063/1.4916826.
[20] K. Toyoki, Y. Shiratsuchi, A. Kobane, C. Mitsumata, Y. Kotani, T. Nakamura, R. Nakatani, Magnetoelectric switching of perpendicular exchange bias in Pt/Co/α-Cr_2O_3/Pt stacked films, Appl. Phys. Lett. 106 (2015) 162404, , https://doi.org/10.1063/1.4918940.
[21] N. Wu, X. He, A.L. Wysocki, U. Lanke, T. Komesu, K.D. Belashchenko, C. Binek, P.A. Dowben, Imaging and control of surface magnetization domains in a magnetoelectric antiferromagnet, Phys. Rev. Lett. 106 (2011) 087202, , https://doi.org/10.1103/PhysRevLett. 106.087202.
[22] K.D. Belashchenko, Equilibrium magnetization at the boundary of a magnetoelectric antiferromagnet, Phys. Rev. Lett. 105 (2010) 147204.
[23] T. Martin, J.C. Anderson, Antiferromagnetic domain switching in Cr_2O_3, IEEE Trans. Magn. 2 (1966) 446–449, https://doi.org/10.1109/TMAG.1966.1065857.
[24] S. Polisetty, J. Scheffler, S. Sahoo, Y. Wang, T. Mukherjee, X. He, C. Binek, Optimization of magneto-optical Kerr setup: analyzing experimental assemblies using Jones matrix formalism, Rev. Sci. Instrum. 79 (2008) 055107, , https://doi.org/10.1063/1.2932445.
[25] J. Wang, C. Binek, Dispersion of electric-field-induced faraday effect in magnetoelectric Cr_2O_3, Phys. Rev. Appl. 5 (2016) 031001.
[26] B.B. Krichevtsov, V.V. Pavlov, R.V. Pisarev, Nonreciprocal optical effects in antiferromagnetic Cr_2O_3 subjected to electric and magnetic fields, Sov. Phys. JETP 67 (1988) 378.
[27] D.S. Kliger, J.W. Lewis, C.E. Randall, Polarized Light in Optics and Spectroscopy, Academic Press, Boston, 1990.
[28] P.M. Oppeneer, Chapter 3 Magneto-optical kerr spectra, Handbook of Magnetic Materials, Elsevier, 2001, pp. 229–422.
[29] C.Y. You, S.C. Shin, Derivation of simplified analytic formulae for magneto-optical Kerr effects, Appl. Phys. Lett. 69 (1996) 1315–1317, https://doi.org/10.1063/1.117579.
[30] J. Wang, Voltage-Controllable Magnetoelectrics: New Thin Film Material and Characterization, The University of Nebraska, Lincoln, Ann Arbor, 2017, p. 430.
[31] T.J. Martin, J.C. Anderson, Magneto-electric annealing effects of Cr_2O_3, Phys. Lett. 11 (1964) 109–110, https://doi.org/10.1016/0031-9163(64)90630-4.
[32] T.J. Moran, J. Nogués, D. Lederman, I.K. Schuller, Perpendicular coupling at Fe–FeF2 interfaces, Appl. Phys. Lett. 72 (1998) 617–619, https://doi.org/10.1063/1.120823.
[33] A. Mahmood, M. Street, W. Echtenkamp, C.P. Kwan, J.P. Bird, C. Binek, Dielectric properties of thin Cr_2O_3 films grown on elemental and oxide metallic substrates, Phys. Rev. Mater. 2 (2018) 044401, , https://doi.org/10.1103/PhysRevMaterials.2.044401.
[34] L. Fallarino, A. Berger, C. Binek, Magnetic field induced switching of the antiferromagnetic order parameter in thin films of magnetoelectric chromia, Phys. Rev. B 91 (2015), https://doi.org/10.1103/PhysRevB.91.054414.
[35] L. Fallarino, A. Berger, C. Binek, Giant temperature dependence of the spin reversal field in magnetoelectric chromia, Appl. Phys. Lett. 104 (2014) 022403, , https://doi.org/10.1063/1.4861780.
[36] T.V.A. Nguyen, Y. Shiratsuchi, A. Kobane, S. Yoshida, R. Nakatani, Magnetic field dependence of threshold electric field for magnetoelectric switching of exchange-bias polarity, J. Appl. Phys. 122 (2017) 073905, , https://doi.org/10.1063/1.4991053.
[37] T.V.A. Nguyen, Y. Shiratsuchi, S. Yonemura, T. Shibata, R. Nakatani, Energy condition of isothermal magnetoelectric switching of perpendicular exchange bias in Pt/Co/Au/Cr2O3/Pt stacked film, J. Appl. Phys. 124 (2018) 233902, , https://doi.org/10.1063/1.5047563.
[38] P. Borisov, T. Ashida, T. Nozaki, M. Sahashi, D. Lederman, Magnetoelectric properties of 500-nm Cr_2O_3 films, Phys. Rev. B 93 (2016) 174415.
[39] X. He, W. Echtenkamp, C. Binek, Scaling of the magnetoelectric effect in chromia thin films, Ferroelectrics 426 (2012) 81–89, https://doi.org/10.1080/00150193.2012.671113.
[40] T. Kosub, M. Kopte, R. Hühne, P. Appel, B. Shields, P. Maletinsky, R. Hübner, M.O. Liedke, J. Fassbender, O.G. Schmidt, D. Makarov, Purely antiferromagnetic magnetoelectric random access memory, Nature Commun. 8 (2017) 13985, https://doi.org/10.1038/ncomms13985.
[41] Y.M. Lu, Y. Choi, C.M. Ortega, X.M. Cheng, J.W. Cai, S.Y. Huang, L. Sun, C.L. Chien, Pt magnetic polarization on $Y_3Fe_5O_{12}$ and magnetotransport characteristics, Phys. Rev. Lett. 110 (2013) 147207, , https://doi.org/10.1103/PhysRevLett. 110.147207.
[42] T. Kosub, M. Kopte, F. Radu, O.G. Schmidt, D. Makarov, All-electric access to the magnetic-field-invariant magnetization of antiferromagnets, Phys. Rev. Lett. 115 (2015) 097201, , https://doi.org/10.1103/PhysRevLett.115.097201.
[43] S. Cao, M. Street, J. Wang, J. Wang, X. Zhang, C. Binek, P.A. Dowben, Magnetization at the interface of Cr_2O_3 and paramagnets with large stoner susceptibility, J. Phys. Condens. Matter 29 (2017) 10LT01.
[44] S.Y. Huang, X. Fan, D. Qu, Y.P. Chen, W.G. Wang, J. Wu, T.Y. Chen, J.Q. Xiao, C.L. Chien, Transport magnetic proximity effects in platinum, Phys. Rev. Lett. 109 (2012) 107204, , https://doi.org/10.1103/PhysRevLett.109.107204.
[45] M. Althammer, S. Meyer, H. Nakayama, M. Schreier, S. Altmannshofer, M. Weiler, H. Huebl, S. Geprägs, M. Opel, R. Gross, D. Meier, C. Klewe, T. Kuschel, J.-M. Schmalhorst, G. Reiss, L. Shen, A. Gupta, Y.-T. Chen, G.E.W. Bauer, E. Saitoh, S.T.B. Goennenwein, Quantitative study of the spin Hall magnetoresistance in ferromagnetic insulator/normal metal hybrids, Phys. Rev. B 87 (2013) 224401, , https://doi.org/10.1103/PhysRevB.87.224401.
[46] Y. Ji, J. Miao, Y.M. Zhu, K.K. Meng, X.G. Xu, J.K. Chen, Y. Wu, Y. Jiang, Negative spin Hall magnetoresistance in antiferromagnetic Cr_2O_3/Ta bilayer at low temperature region, Appl. Phys. Lett. 112 (2018) 232404, , https://doi.org/10.1063/1.5026555.
[47] H. Nakayama, M. Althammer, Y.T. Chen, K. Uchida, Y. Kajiwara, D. Kikuchi, T. Ohtani, S. Geprägs, M. Opel, S. Takahashi, R. Gross, G.E.W. Bauer, S.T.B. Goennenwein, E. Saitoh, Spin Hall magnetoresistance induced by a nonequilibrium proximity effect, Phys. Rev. Lett. 110 (2013) 206601, , https://doi.org/10.1103/PhysRevLett. 110.206601.
[48] Y.-T. Chen, S. Takahashi, H. Nakayama, M. Althammer, S.T.B. Goennenwein, E. Saitoh, G.E.W. Bauer, Theory of spin Hall magnetoresistance, Phys. Rev. B 87 (2013) 144411, , https://doi.org/10.1103/PhysRevB.87.144411.
[49] R. Schlitz, T. Kosub, A. Thomas, S. Fabretti, K. Nielsch, D. Makarov, S.T.B. Goennenwein, Evolution of the spin hall magnetoresistance in Cr_2O_3/Pt bilayers close to the Néel temperature, Appl. Phys. Lett. 112 (2018) 132401, , https://doi.org/10.1063/1.5019934.
[50] S.P. Pati, M. Al-Mahdawi, S. Ye, Y. Shiokawa, T. Nozaki, M. Sahashi, Finite-size scaling effect on Néel temperature of antiferromagnetic Cr_2O_3 (0001) films in exchange-coupled heterostructures, Phys. Rev. B 94 (2016) 224417, , https://doi.org/10.1103/PhysRevB.94.224417.